Kaihui Cui, Tianqi Liao, Chen Qiu, Hua Chen* and Junwen Zhou*

Microwave-induced heating behavior of Y-TZP ceramics under multiphysics system

https://doi.org/10.1515/gps-2020-0013
Received August 16, 2019; accepted October 22, 2019.

Abstract: This paper aims to investigate the heating behaviors of Y-TZP arrays under microwave irradiation. In this study, a three-dimensional numerical model of the microwave heating system was developed by COMSOL Multiphysics software. The numerical model was verified by microwave heating experiment, and the average root means square errors (RMSE) between the simulation and experimental data also confirmed the reliability of the model. The varying position and arrays of materials were applied to predict and visualize the three-dimensional distribution of the electromagnetic field and temperature during the microwave heating process. The results show that the temperature field distribution in microwave cavity was highly sensitive to the dielectric materials, the arrangement of the Y-TZP array interfered with the distribution of standing waves. The results can serve as references for the study to design and optimize the ceramic's application in terms of microwave heating.

Keywords: microwave heating; Y-TZP ceramic; missing array element; COMSOL Multiphysics

*** Corresponding authors: Hua Chen and Junwen Zhou,** Key Laboratory of Unconventional Metallurgy, Ministry of Education, Kunming University of Science and Technology, Kunming 650093, China; Department of Metallurgical and Energy Engineering, Kunming University of Science and Technology, Kunming 650093, China; Department of Science, Kunming University of Science and Technology, Kunming 650093, China,
e-mail: 93056460@qq.com (Hua Chen),
754400566@qq.com (Junwen Zhou)
Kaihui Cui and Tianqi Liao, Key Laboratory of Unconventional Metallurgy, Ministry of Education, Kunming University of Science and Technology, Kunming 650093, China; Department of Metallurgical and Energy Engineering, Kunming University of Science and Technology, Kunming 650093, China
Chen Qiu, Department of Mechanical and Electrical Engineer, Kunming University of Science and Technology, Kunming 650093, Yunnan, China

1 Introduction

Biomass is an abundant green renewable resource that can be partially substituted for fossil energy. Biomass pyrolysis is one way of thermochemical conversion, producing plenty of chemical compounds: permanent gas, pyrolytic liquid (tar or bio-oil) and char [1]. Fast pyrolysis and carbonization, two main pyrolysis processes, are of interest: fast pyrolysis [2] and carbonization [3] for maximizing the bio-oil and the charcoal production, respectively. Fast pyrolysis offers the advantage of generating a liquid fuel (bio-oil), which can substitute for fuel oil or diesel in many static facilities including boilers, furnaces, engines and turbines for electricity generation. To improve the quality of the product, biomass rapid pyrolysis should be carried out with a quite high heating rate of the solid up to a moderate temperature (around 500°C) and with short residence time of the vapor-phase products [4].

Microwave dielectric heating has the potential to be rapid and energy-efficient [5,6] and has been widely applied in heterogeneous gas-phase catalytic systems and a variety of other fields including food processing [7], wood drying, plastic and rubber processing as well as curing and preheating of ceramics. In contrast with conventional heating, the dielectric material (microwave-absorbing material) can quickly absorb microwave energy and convert it into thermal energy in the electromagnetic field [8]. It presents numerous advantages such as higher heating rates, selective heating, a better control of the heating process, reduced equipment size and reduced waste. As biomass materials are scarce receptors of microwave energy, which are hardly heated. But the added dielectric material acting as "microwave receptors" highly improves the conversion rate. In the fast pyrolysis process, excellent thermal conductive materials are indispensable as transfer carriers that can make biomass rapidly heated to moderate temperatures [9].

The zirconia ceramic (Y-TZP) material has good microwave absorbance, thermal stability and chemical stability without reacting with the sintered body. And it has good thermal shock resistance to be an ideal setter material. Guo et al. [10] reported the mixture of coconut-based activated carbon, coke and graphite has a better microwave absorbance than oxidized ilmenite. Therefore, it could be

speculated that Y-TZP, as a stable dielectric material, can be mixed with biomass to improve the microwave heating rate, and the mixture is likely to be a good microwave-absorption material, i.e., the rapid pyrolysis of biomass can be realized by absorbing the heat energy exchanged from the external surface of zirconia ceramic [11,12].

Experiments are of great importance for investigating microwave heating, however, the electromagnetic evolution during heating cannot be physically measured. Furthermore, it is hard to predict the internal thermal field of heated material [13,14]. Over the last two decades, numerical simulation has become a promising tool to quantize and visualize the complex microwave heating process. As a powerful software package, COMSOL Multiphysics is feasible to simulate microwave heating by coupling electromagnetic and heat transfer physics [15-17]. The field of microwave heating has attracted a lot of researches with numerical modeling and analysis techniques. Despite extensive research, the complexity of interactions among multimode cavity microwave and materials impeded the development of reliable theoretical models. Most of the microwave simulation researches focused on variables such as microwave frequency, power input, heating time, sample size and so on [18,19]. However, there are few studies focusing on the effect of dielectric material physical array distribution of absorbance. From the perspective of efficient usage of microwave energy and cost control, it is more feasible to adjust the material's position and size to achieve optimal microwave absorbance. Therefore, accurate estimating of the electromagnetic-thermal distribution of Y-TZP in a microwave cavity is critical to microwave processing.

The main purpose of this paper is to establish a coupled model of electromagnetic and heat transfer to investigate the thermal behavior of Y-TZP under microwave irradiation. The specific achievements of this research work are: (i). A numerical model of the microwave heating system was developed by COMSOL Multiphysics software (ii). The model was verified through the microwave heating experiments. (iii). The three-dimensional distribution of the electromagnetic field and temperature was modeled based on different parameters (sample height, sample periodic array distribution, missing array distribution). This study will provide the basis for parameter optimization in the microwave heating process design.

2 Model formulation

2.1 Geometric model

The microwave heating system in this work is designed and fabricated by the Key Laboratory of Unconventional Metallurgy of the Ministry of Education, Kunming University of Science and Technology (Figure 1). The geometric model

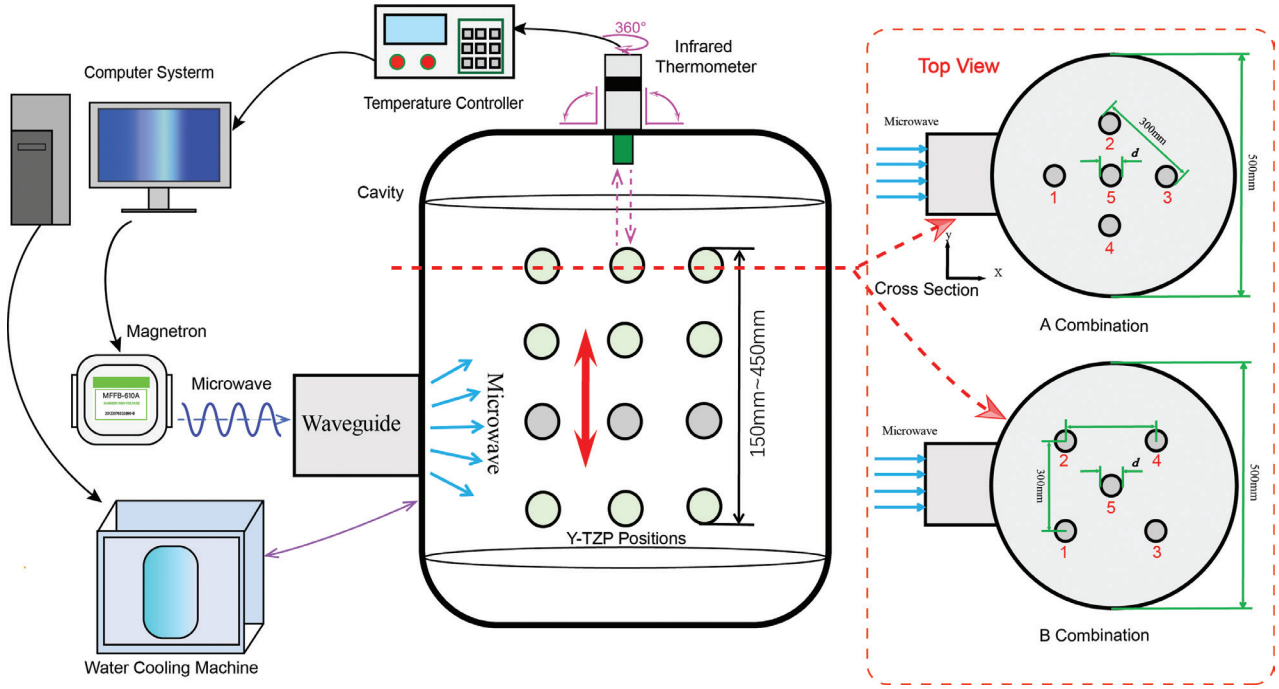

Figure 1: Schematic diagram of the geometric model.

developed in COMSOL Multiphysics was the same as the size of the experimental device, and the global model size parameters shown in Table 1. The computer-controlled magnetron generated microwave energy and supplied into the microwave cavity through the waveguide (x-direction). The mode of the microwave was assumed to excite the TE_{10} mode wave at 2.45 GHz frequency. The temperature of the material was measured by an infrared thermometer, all sensors use the same mounting hardware and (Raytek) DataTemp Multidrop software. The infrared thermometer converted the radiant energy (infrared rays) into an electrical signal, which reflected by material. The infrared thermometer was aligned with the material, and the angle of the infrared thermometer was adjusted according to the position of material.

2.2 Governing equations and boundary conditions

The COMSOL simulation design for the microwave cavity is the solution of Maxwell's equations under certain boundary conditions and excitation conditions. The Maxwell's equations describing the essential characteristics of electromagnetic fields listed in Table 2.

The energy absorbed (P_{ab}) by the material is converted as follows:

$$P_{ab} = \frac{\omega \varepsilon_0 \varepsilon_r'' \left| E \right|^2}{2} \tag{1}$$

The dielectric permittivity (ε_r) of the material is expressed in complex form as:

$$\varepsilon_r = \varepsilon_r' - j\varepsilon_r'' \tag{2}$$

where $j = \sqrt{-1}$, and ε_r' is the dielectric constant (F/m) that reflects the capacity of the material to store electromagnetic energy, whereas ε_r'' *is* the loss factor that dominates the conversion of electromagnetic energy into heat.

By eliminating E from Maxwell equations, the following Helmholtz equation of electric field vector fluctuation can be obtained:

$$\nabla \times \left(\mu_r^{-1} \nabla \times \boldsymbol{E} \right) - k_0^2 \left(\varepsilon_r - \frac{j\sigma}{\omega \varepsilon_0} \right) \boldsymbol{E} = 0 \tag{3}$$

where wave number in free space, k_0 is defined as:

$$k_0 = \frac{\omega}{c_0} \tag{4}$$

where c_0 is the speed of light in vacuum.

The thermal and heat transfer conditions for the Y-TZP ceramics applied according to Eq. 5. This equation coupled the electromagnetic heating module of COMSOL with those of the heat transfer by Fourier's energy balance equation as follows:

$$\rho C_P \frac{\partial T}{\partial t} = \nabla \cdot \left(k \nabla T \right) + Q \tag{5}$$

where ρ is the density (kg/m^3), C_P is the specific heat capacity (J/(kg · K)), k is the thermal conductivity (W/(m · K)) of the material, T is the temperature (K) and Q is the heat source.

Table 1: Global model parameters.

	Depth (mm)	Width (mm)	Height (mm)	Radius (mm)
Microwave cavity	600	–	–	250
Waveguide	54.61	109.22	180	–
Y-TZP ceramics	–	–	150 to 450	20

Table 2: Maxwell's equations.

Maxwell's equations	Governing laws	Terms
$\nabla \times H = -j\omega\varepsilon_0\varepsilon^* E$	Maxwell-Ampere's law	E – electric field intensity
$\nabla \times E = -j\omega\mu H$	Faraday's law	H – magnetic field intensity
$\nabla \cdot (\varepsilon_r E) = 0$	Gauss law e electric	ω – angular frequency
$\nabla \cdot H = 0$	Gauss law e magnetic fields	μ – permeability
		ε_0 – free space permittivity
		ε_r – complex dielectric permittivity

The heat source (Q) in Eq. 5 represents the electromagnetic losses (Q_l), due to an electrical and magnetic field and is given by Ref.

$$Q_l = Q_{rh} + Q_{ml} \tag{6}$$

where the resistive losses (Q_{rh}) is given by:

$$Q_{rh} = \frac{1}{2} Re\left(J \cdot E^{\star}\right) \tag{7}$$

and magnetic losses (Q_{ml}) is given by:

$$Q_{ml} = \frac{1}{2} Re\left(i\omega B \cdot H^{\star}\right) \tag{8}$$

A perfect electrical conductor boundary condition was defined for the microwave cavity walls and waveguide, whereas the perfect magnetic conductor boundary condition ($n \times H = 0$) assigned for the symmetry boundaries.

$$\sqrt{\frac{\mu_0 \mu_r}{\varepsilon_0 \varepsilon_r - j\frac{\sigma}{\omega}}}\, n \times H + E - \left(n \cdot E\right) n = \left(n \cdot E_s\right) n - E_s \tag{9}$$

The properties in Eq. 9 such as relative permittivity (ε_r), relative permeability (μ_r), and electrical conductivity (σ) are all taken from the material. The symmetry boundary considers that there is no heat flux across the boundary and that the boundaries are thermally well insulated which is defined by the following equation:

$$n \cdot \left(k \nabla T\right) = 0 \tag{10}$$

2.3 Material

The zirconia ceramics (Y-TZP) was supplied by Jiangxi Pingxiang Baitian New Material Co., Ltd. The typical Purity Data (%) of zirconia ceramics were determined by Foshan Ceramics Research Institue Co, Ltd, and the results are as follows: 94.75 of ZrO_2, 4.90% of Y_2O_3, 0.30% of Al_2O_3, 0.01% of Fe_2O_3 and 0.01% of Na_2O. The thermal and electric properties of the Y-TZP shown in Table 3.

2.4 Mesh size

The mesh element sizes differed based on the problem definition and the effect of various parameters studied in this paper, free tetrahedral mesh element selected for the whole geometry. The number of tetrahedral and triangular elements was 191896 and 8764. However, to ensure the simulation converges and to get an accurate result, the maximum mesh element size in the Y-TZP was refined to 4.7 mm, while a predefined normal mesh element size of 24 mm selected for the multimode cavity, reactor, and waveguide.

Grid Element Quality (MEQ) measures the morphological regularity of mesh elements, which is essential for model validation, and lower MEQ poses problems for model convergence, the model is considered reliable when MEQ > 0.3 [21]. The visualization and statistical statistics of MEQ are shown in Figure 2, respectively. It can be clearly found that the quality of the model unit is satisfactory, and the model is considered to be reliable.

Table 3: Thermal and electric properties of Y-TZP used for simulation work.

Material properties	Unit	Values		
		Y-TZP	Copper[b]	Air[b]
Relative permittivity	1	27-1.112*j [a,c]	1	1
Relative permeability	1	1	1	1
Electrical conductivity	S/m	0.056	5.998e7	0
Thermal conductivity	W/m K	2[c]	400	0
Density	kg/m^3	6030[c]	8960	–

[a] Taken from Ref [20].
[b] Taken from COMSOL built-in material library.
[c] This study.

2.5 Assumptions

Even though there has been rapid advancement in the computational software to provide accurate results that can be applied in real a case with maximum confidence, still one cannot avoid numerical errors arising from the sparse discretization of time and space domain. Hence, assumptions need to be made in order to simplify the problem and reduce computational time.

1. Constant dielectric properties and thermal conductivity properties were applied when solving the heat transfer equations.
2. No heat transfer was considered from the surrounding cavity and environment.
3. The mass transfer and shrinkage of Y-TZP ceramics were assumed negligible.

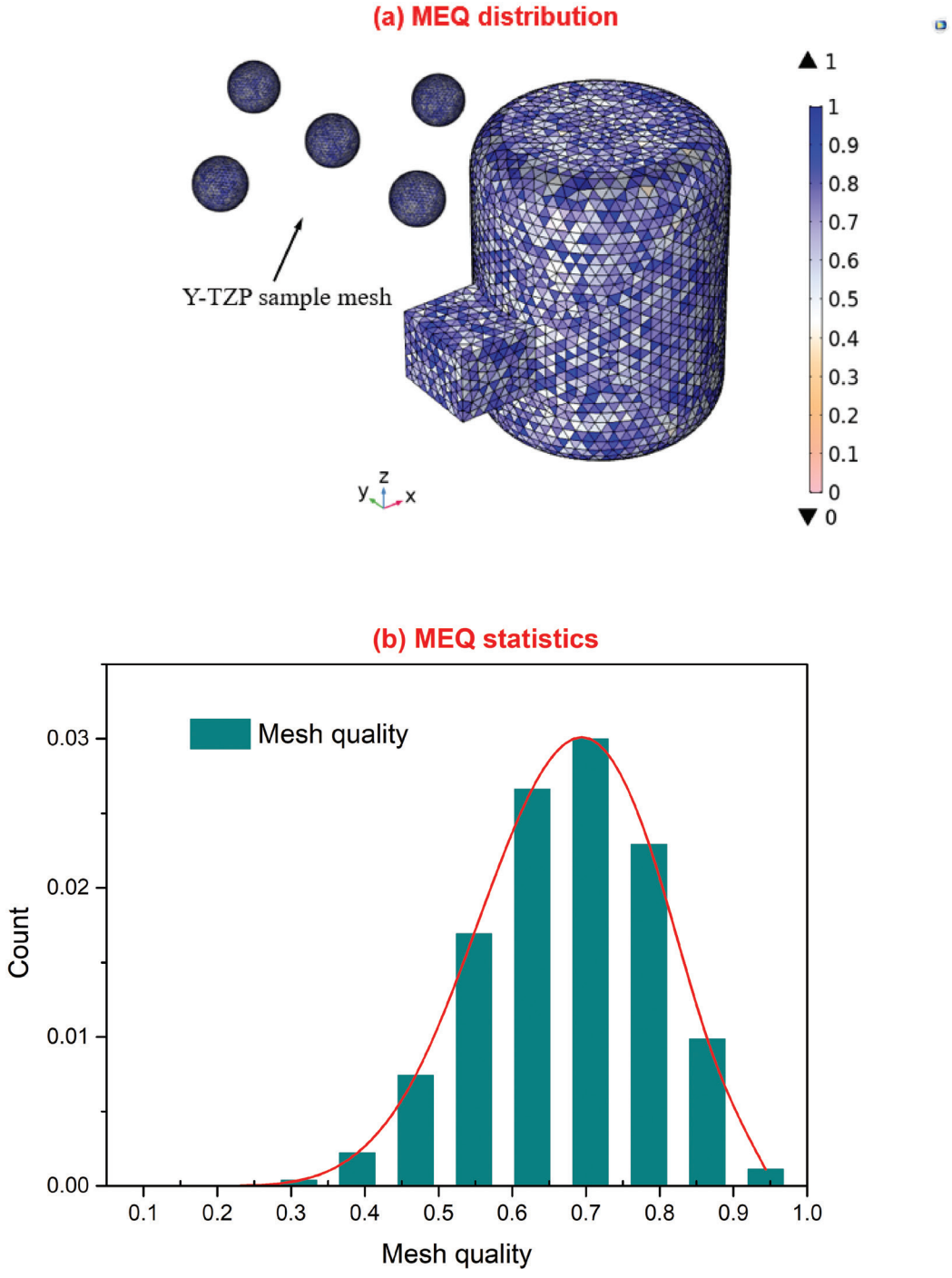

Figure 2: Construction of resonant cavity grid: (a) the visualization of MEQ distribution in model, (b) the MEQ statistics in the model.

4. Detailed simulation on how the energy was extracted from the waveguide into the cavity was not modeled.
5. The waveguide port was excited by a transverse electric field in the x-direction.
6. The quartz glass plate was not modeled because it was transparent to the microwave.

3 Experimental work and validation

Upon entering system geometry and defining the boundary and initial conditions in COMSOL Multiphysics, the partial differential equation solve by the Finite Element Method. The calculation time range was from 0 to 300 with each step of 30 s. The whole process of

keeping applying a power of 1000 W and a frequency of 2.45 GHz. There are two combinations in this study, A and B, as shown in Figure 1. Y-TZP ceramics were placed in the x and y planes component along the microwave excitation direction. Based on the combinations, the height of the Y-TZP varying along the z component red line, moved from 150 to 450 with a step of 100 mm.

To evaluate the model accuracy between the experimental and simulated temperature data, the root means square error (*RMSE*) is defined as:

$$RMSE = \sqrt{\frac{1}{n}\sum_{i=1}^{n}\left(T_s - T_e\right)^2} \tag{11}$$

where T_e and T_s are the experimental date and simulated temperature, respectively.

The numerical model can record the temperature at any position of the sample. Figure 3 shows the simulated temperature and experimental data at the upper surface of the Y-TZP ceramics. It can be seen that agreement between the experiments and simulations was quite reasonable, and the *RMSE* range from 50.34 to 53.38 K. This error could be attributed to the assumption of monochromatic and material properties, e.g., a magnetron operates at a range of frequencies, the permittivity of Y-TZP also could cause the deviations of simulation temperature from experimental data. Agreement between the experiments and simulations is quite reasonable due to this is a complex couple microwave heating simulation, although the errors are inevitable, the mathematical model is still reliable [22].

4 Results and discussion

4.1 Effect on Y-TZP height in the microwave cavity

The distribution of the electric field and temperature distribution in the cavity are exhibited in Figures 4 and 5, rainbow maps are used in profiles, where red represents a high-intensity region and blue is a low-intensity region. One of the caused for non-uniform heating of Y-TZP subjected was the extremely uneven electric field distribution within the cavity, as shown by the electric field in the z component and y component. The effect of the materials' height on temperature profile was clearly, the heating rate got modified with height varying, it means that the Y-TZP

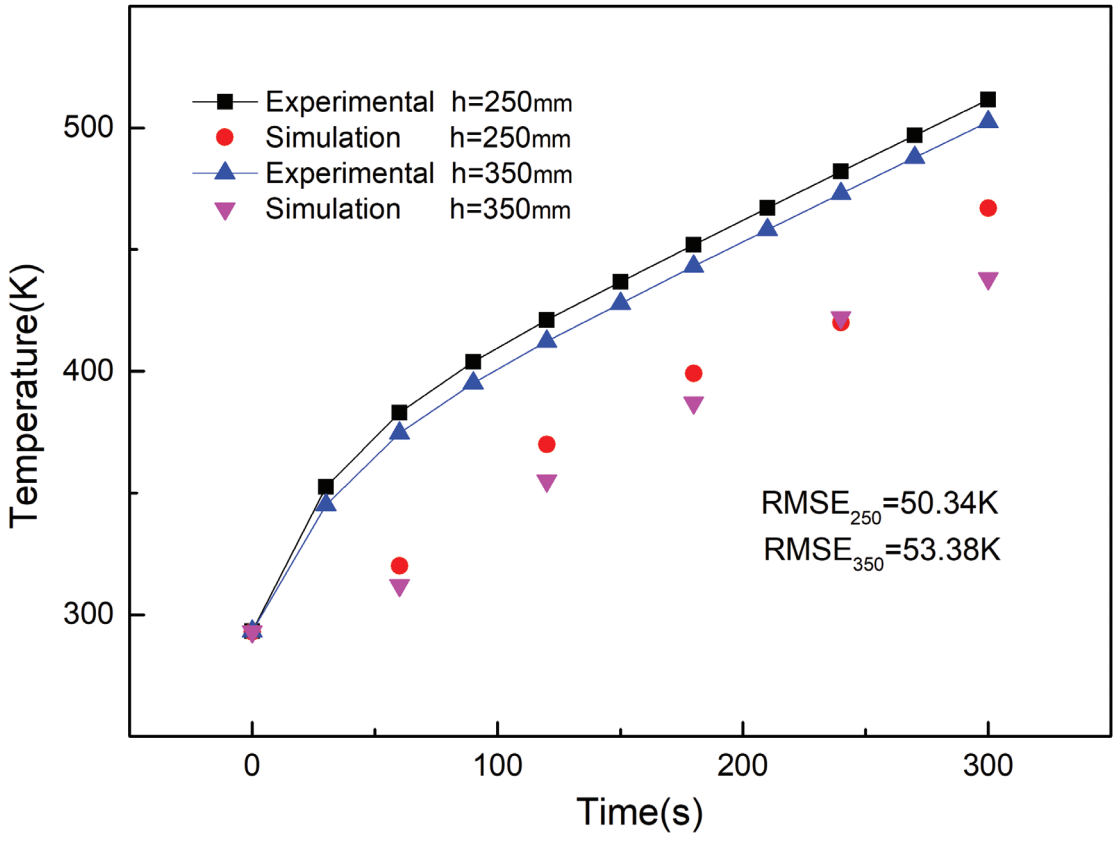

Figure 3: Comparison of the experimental and simulated temperature evolution of Y-TZP, h = 250 mm and h = 350 mm.

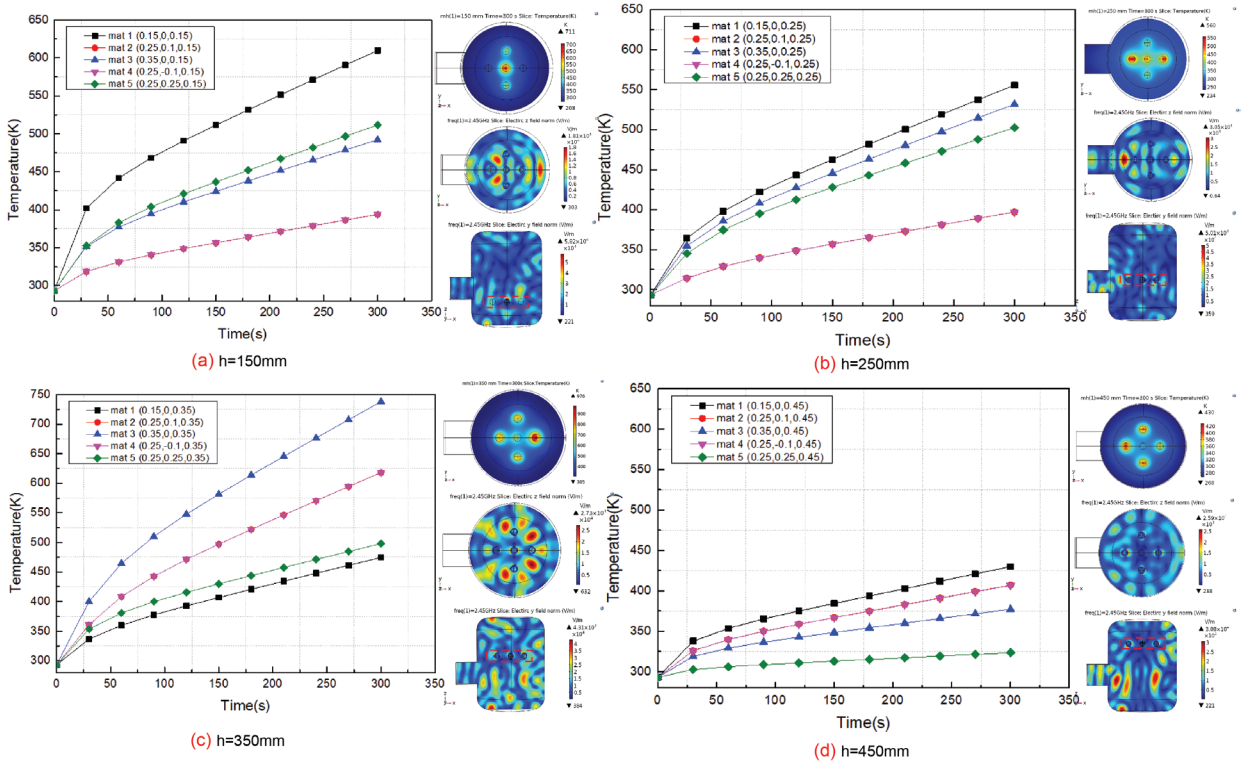

Figure 4: Influence of the variations of height on the heating rate and temperature distribution, combination A.

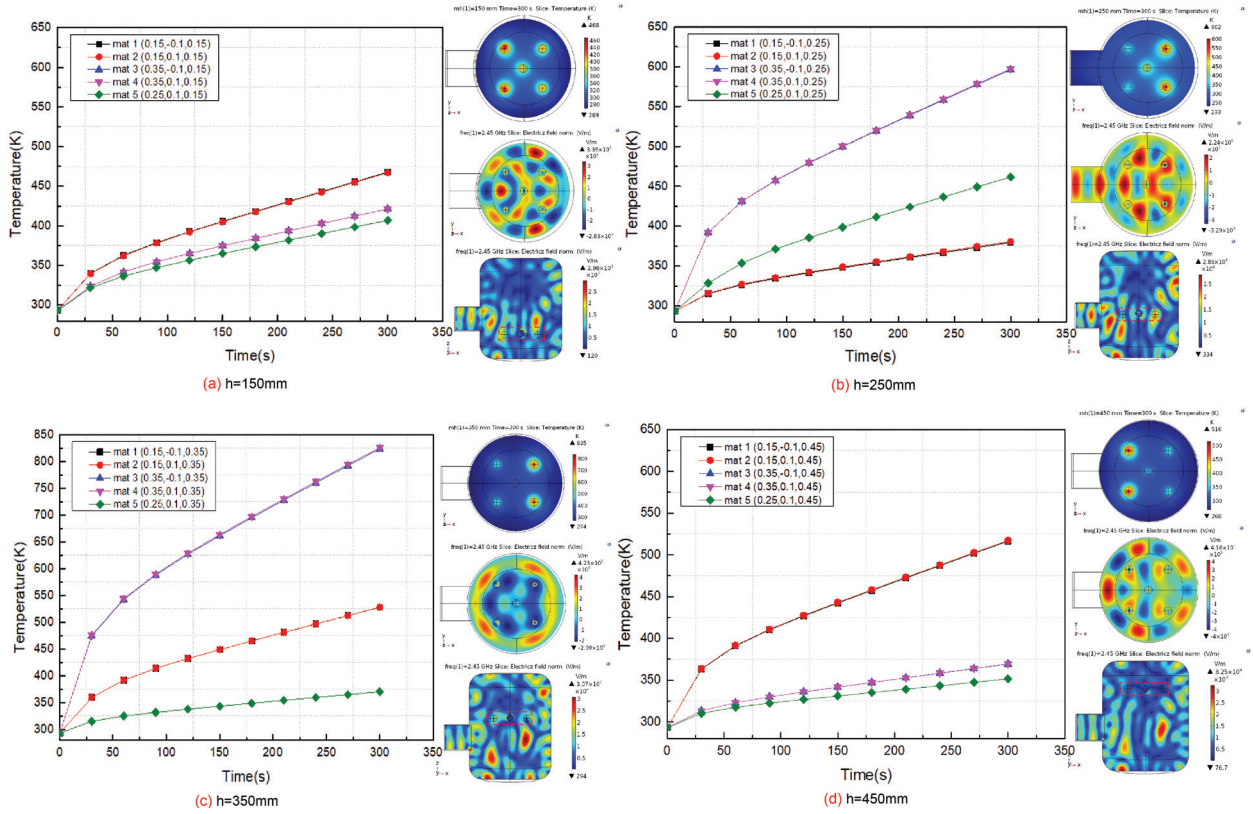

Figure 5: Influence of the variations of height on the heating rate and temperature distribution, combination B.

position affected the electric fields. The heating curve shows the temperature in the center of the Y-TZP for heating 300 s. Interesting, compared with two combinations that there has a common characteristic, the heating rate was the fastest at first 27 s, and then the heating rate became slower. At the initial stage of microwave heating, with heating process, the polar molecules to rotate and realign to alternate electromagnetic field, a multitude of molecular rotation and collision generate friction thereby resulting in heat quickly. The dielectric loss factor changes and stabilizes after reaching the critical temperature, which also makes the microwave heating rate tend to be stable [23].

It is widely accepted that the heating rate of the material greatly depends on the electric field intensity. Higher electric intensity leads to more microwave absorption [24,25]. The electric field diagrams of Y-TZP moved from the bottom of the microwave cavity to the top, the red area represents the high intensity, and the blue indicates the low intensity. Obviously, the addition of Y-TZP affected the distribution of standing waves, it caused a non-uniform electric field distribution in the microwave cavity. Y-TZP has a better microwave-absorbing effect, where located in a strong electric field area. Furthermore, it caused thermal runaway because of the large gradient of the field strength difference around the Y-TZP.

The non-uniform heat generation with microwave irradiation due to the spatial variations of the electromagnetic field or non-homogeneous distribution of material. The high-temperature areas in the material are usually known as 'hot spots' [22]. It can be seen from the temperature diagram that the temperature distribution was significantly affected by the materials' height. With the materials' height varying, there was a vast difference between the highest temperature (hot spot) and the lowest temperature (cold spot). Both combinations' hot spots were around h = 350 mm, the hot spot of combination A reached to 748 K, and the combination B was 825 K. Unusually, the hot spot not only appeared close to the waveguide but also appeared in the distance.

4.2 Effect of global total cumulative energy

After the height of the Y-TZP ceramics reached to h = 220 mm from the bottom of the cavity, the heating curve tended to be more consistent., combination B of temperature was generally better than combination A in general. Hence, this section focus on an analysis of the arrangement of combination B. In order to be more optimized and more precise, parametric scanning was defined in the range from 320 to 370 mm, with a step length of 10 mm. The profiles of simulation results limited the temperature legend boundary, plan view of the temperature distribution (Figure 6) shows the hot spot occurred at h = 340 mm, where the center position has the highest temperature.

There is a significant gradient change in energy accumulation at different heights as exhibited in Figure 7.

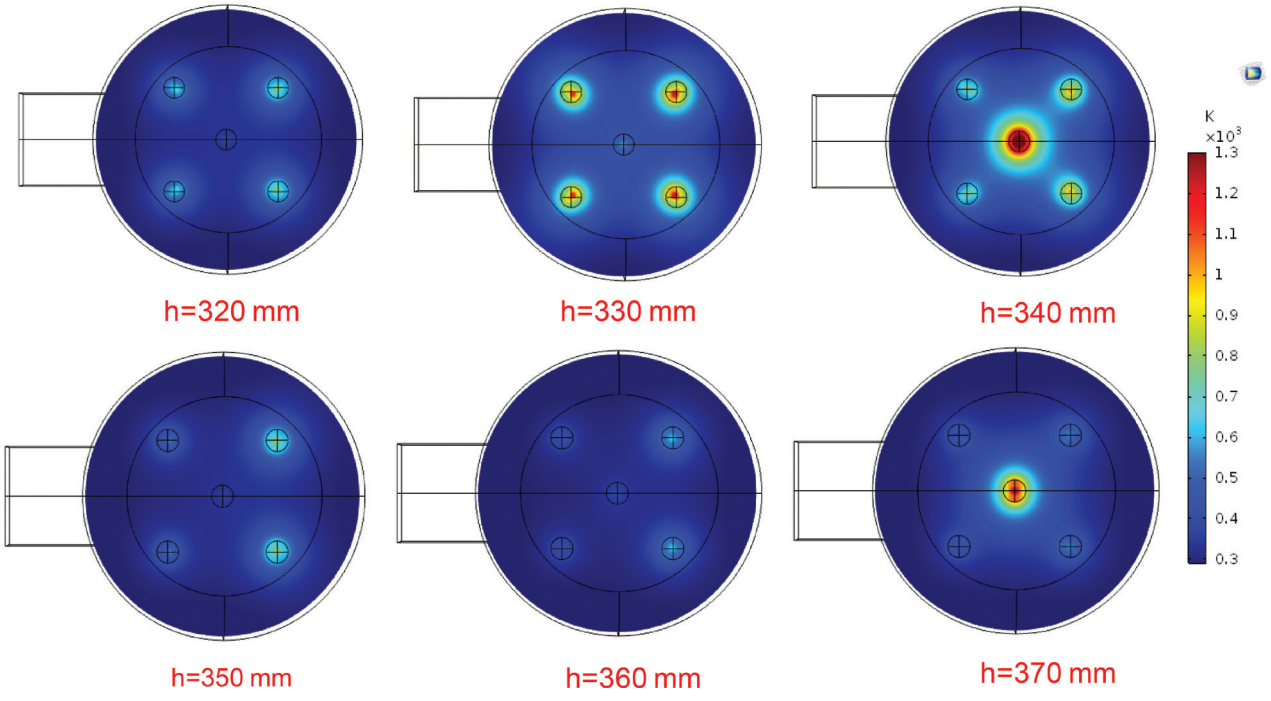

Figure 6: The temperature distribution profiles of combination B, height range from 320 to 370 mm.

The energy accumulation effect increased firstly and then decreased with the height increased. The curves followed the great trend at the height of 330 and 340 mm. Before 27 s, the speed of the overall geometric energy gathered increased, and the maximum rate occurred at h = 340 mm, where is consistent with the thermal field distribution in Figure 6, i.e., the interaction of the electric field with Y-TZP has a best coupled [26,27].

4.3 Effect of a missing array element of the sample

Through the above calculation work, the heating effect was best when Y-TZP was located at h = 340 mm. Deleted elements of the initial symmetrical Y-TZP, the heating curve of the missing array is shown in Figure 8, the solid line in the profile represents the heating curve of the original periodic array, and the dashed line represents the heating curve after the missing element; *mat1, mat2. mat3, mat4,* and *mat5* represent the position of Y-TZP, the temperature monitoring points were the three-dimensional center intercept point of the Y-TZP.

The heating curves of the missing array are exhibit in Figure 8. The heating rate of the missing array model was significantly improved. For combination A, missing the *mat1* near the waveguide (Figure 8a) or missing the *mat3* far away from the waveguide (Figure 8b), the temperature of the outer layer increased 100~200 K in generally. removed *mat1*, the temperature of *mat3* can reach to 900 K in 300 s; For combination B, removed *mat1* and *mat2* (Figure 8c), the temperature of *mat5* increased 150 K than before, but there was a little change for *mat3* and *mat4*. When *mat3* and *mat4* were removed (Figure 8d), the temperature has greatly improved than before. With microwave irradiation for 300 s, all the materials' temperature rose more than 870 K, especially the center *mat5* reached to 950 K.

The geometrical simulation and experimental data are shown in Figure 9, which used the arrangement of Y-TZP in Figure 8d. There were two spherical symmetrical distributions near the waveguide, and another one located on the central line of the waveguide port, the missing array presented as a triangular, and the infrared thermocouple aligned *mat1* for temperature measurement. The experimental results were agreement to the simulated data, the error of the model has described in section 3. The array of Y-TZP varying resulted in more microwave energy converted into heat, and the Y-TZP reached the specified temperature in a shorter time.

4.4 Equivalent circuit analysis

According to the characteristics of electric field distribution in the cavity, placed the Y-TZP at the high electric intensity fields, the optimal coupling results can be obtained by

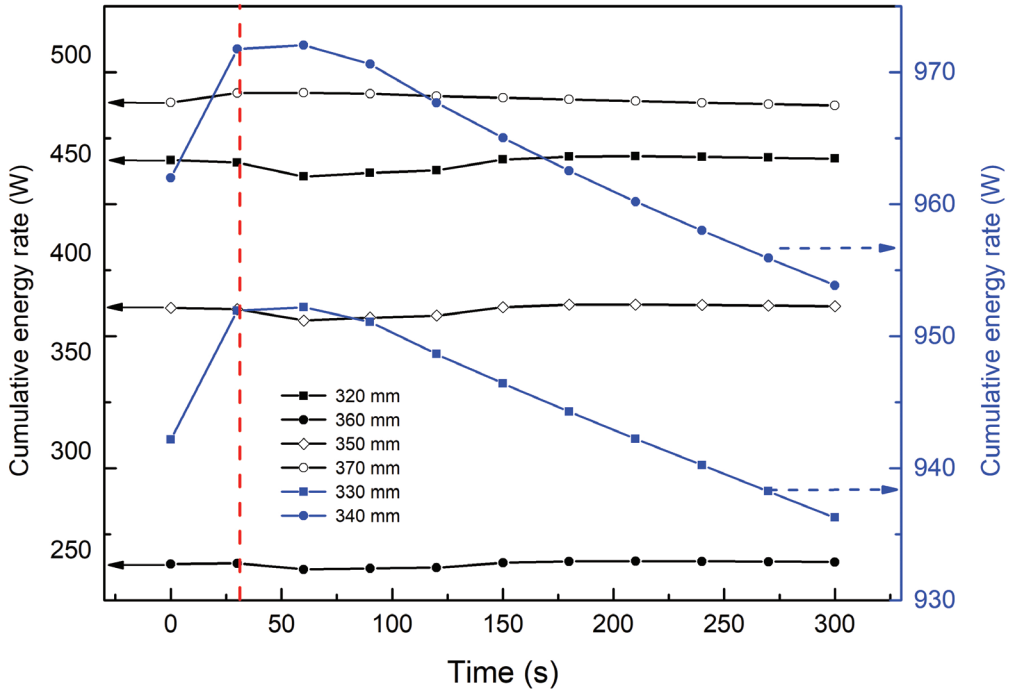

Figure 7: Global total cumulative energy rate (W), height range from 320 to 370 mm.

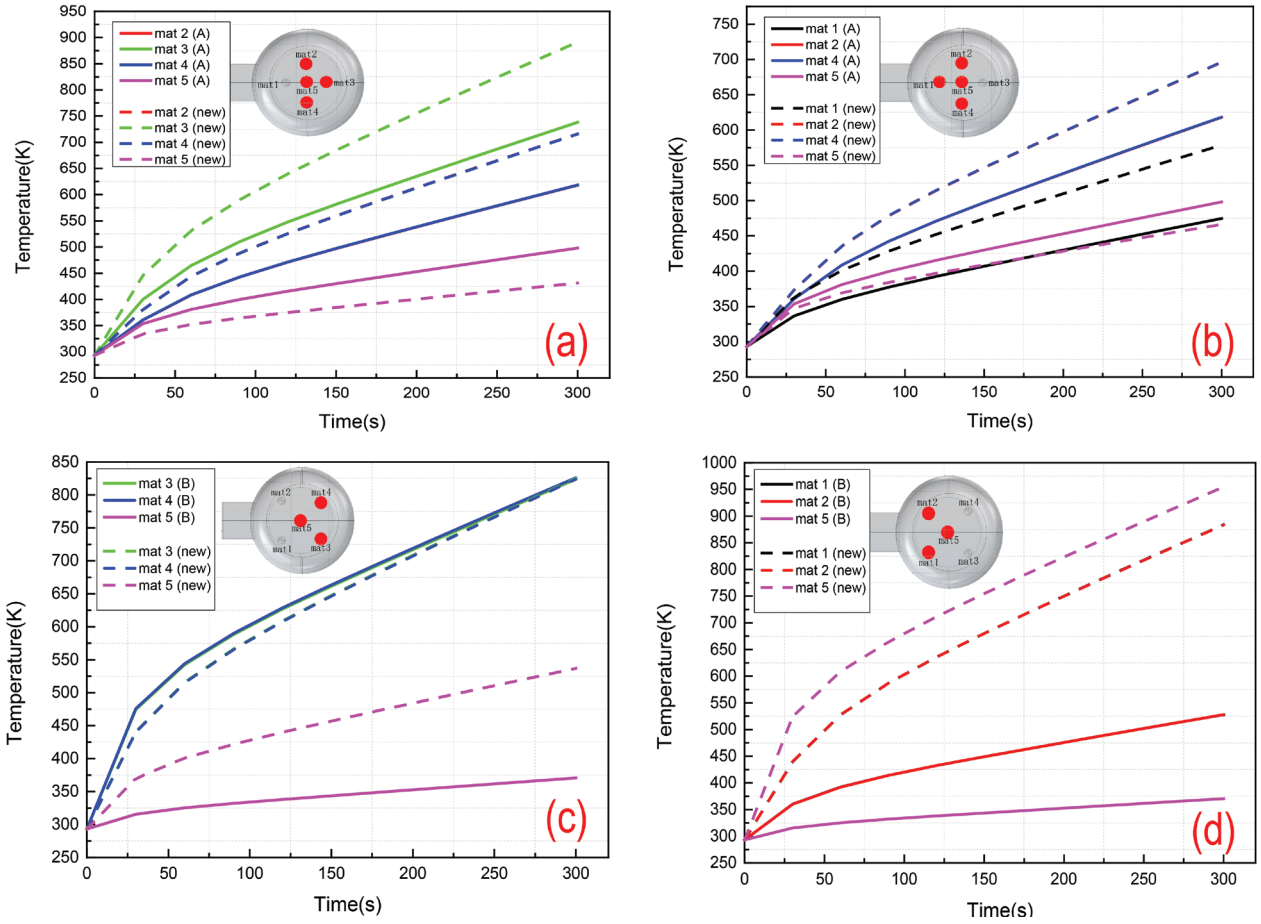

Figure 8: The heating curve for missing array of Y-TZP, at h = 340 mm.

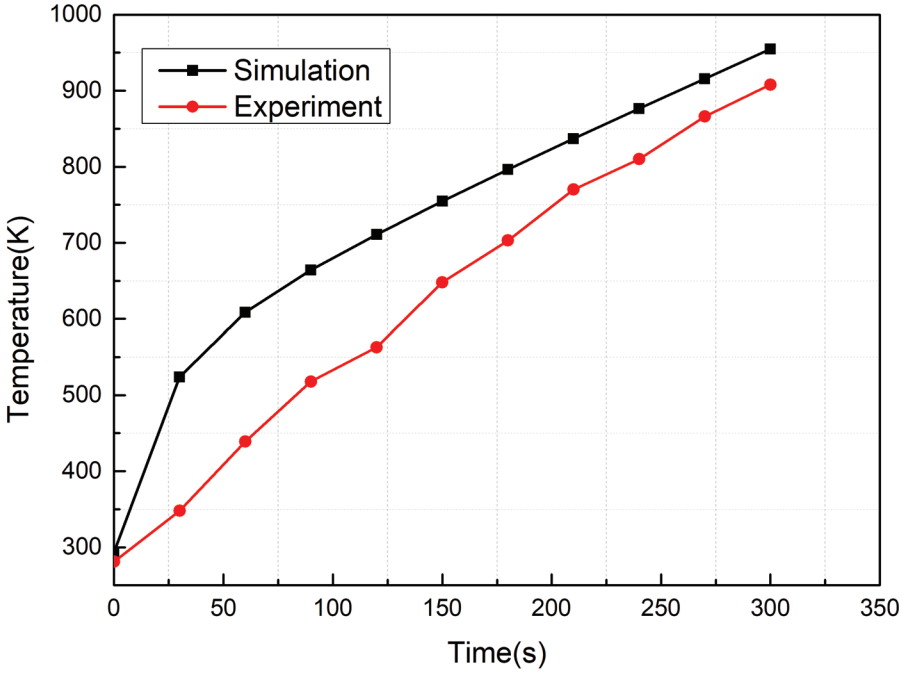

Figure 9: Comparison of the experimental and simulated temperature evolution of Y-TZP, at h = 340 mm.

microwave irradiation. The great absorption of Y-TZP achieved at Y-TZP near waveguide and h = 340 mm. The equivalent circuit was used to analysis the microwave-absorbing of *mat1*, *mat2* was better than *mat3*, *mat4*.

$$R_a = R_{L1} + \frac{R_3 R_4}{R_3 + R_4} + R_5 \tag{12}$$

$$R_b = R_{L2} + \frac{R_1 R_2}{R_1 + R_2} + R_5 \tag{13}$$

$$W = \frac{U^2}{R} t \tag{14}$$

In the equivalent circuit, the microwave considered as the current, and the Y-TZP considered as the resistors. Defined the air dielectric loss and the reflection of the metal wall as R_L, *mat1*, *mat2*, *mat3*, *mat4*, and *mat5* represents the resistors R_1, R_2, R_3, R_4, R_5, respectively. For the current passed through the resistor, following the principle of energy conservation, the resistor blocked and reduced a part of the current and converted into heat. As shown in Figure 10, for Y-TZP neared to the waveguide, the microwave transmission distance increased, it led the value (R_L) of air dielectric loss and the reflection loss became larger, i.e., the value of R_{L1} was higher than R_{L2}. The initial value was regarded as the same current in Eq. 13, R_1, R_2, R_3, and R_4 were connected in parallel with the circuit, the total value of R_b was less than R_a. With current passing through R_a, R_b, resistance loss and converted into more thermal energy ($W_b > W_a$).

5 Conclusions

In this paper, using COMSOL Multiphysics software simulated the microwave heating the array of Y-TZP, the numerical coupled electromagnetic and heat transfer equations were successfully solved. This model was verified by the microwave heating experiment and the average root means square errors, and the simulated temperature obtained has a good agreement with the experimental data. The varying parameters of Y-TZP were applied to visualize the three-dimensional distribution of the electromagnetic field and temperature during microwave heating process. The following results are obtained:

(1) The varying parameters of Y-TZP affected temperature distribution and thermal behavior.
(2) The arrangement of the Y-TZP array interfered with the distribution of standing waves.
(3) The missing array elements have a great influence on Y-TZP microwave absorbing.

Among the aspects that have not been given consideration in this study and whose importance should be evaluated by the development of more advanced models. A further analysis of the influences of the medium dielectric properties and the size/shape of both materials are also needed for the successive steps of technology

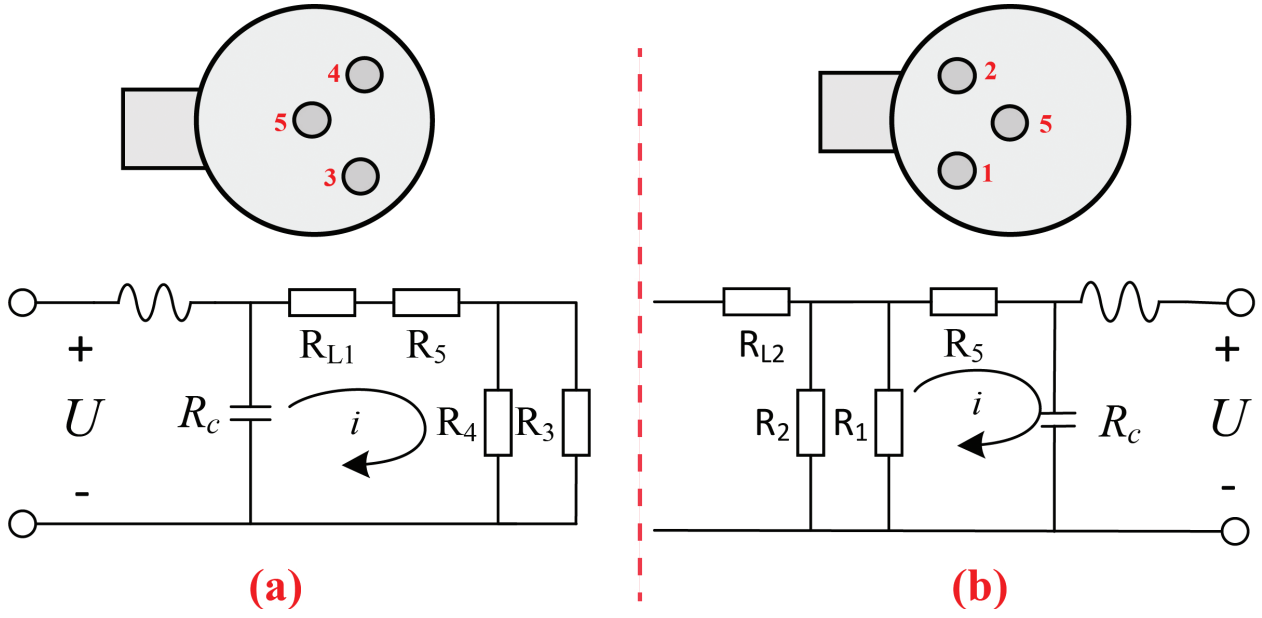

Figure 10: Schematic diagram of equivalent impedance matching.

design and optimization. Finally, detailed measurements of the field variables and properties of material are needed for improving the knowledge of the process fundamentals and for experimental validation of comprehensive models.

Acknowledgments: This work was supported by the National Natural Science Foundation of China (Nos. 61764008 and 21966019). Analysis and Testing Foundation of Kunming University of Science and Technology (No.2018M20172202030).

Disclosure statement: No potential conflict of interest was reported by the authors.

References

[1] Di Blasi C., Modeling chemical and physical processes of wood and biomass pyrolysis. Prog. Energ. Combust., 2008, 34(1), 47-90.

[2] Bridgwater A.V., Renewable fuels and chemicals by thermal processing of biomass. Chem. Eng. J., 2003, 91(2-3), 87-102.

[3] Antal M.A., Grønli M., The Art, Science, and Technology of Charcoal Production. Ind. Eng. Chem. Res., 2003, 42(8), 1619-1640.

[4] Press C., Fast Pyrolysis of Biomass. J. Anal. Appl. Pyrol., 2017, 6(2), 95-135.

[5] McWilliams B., Yu J., Zavaliangos A., Fully coupled thermal-electric-sintering simulation of electric field assisted sintering of net-shape compacts. J. Mater. Sci., 2015, 50(2), 519-530.

[6] Kell R.C., Greenham A.C., Olds G.C.E., High-Permittivity Temperature-Stable Ceramic Dielectrics with Low Microwave Loss. J. Am. Ceram. Soc., 2006, 56(7), 352-354.

[7] Motasemi F., Afzal M.T., A review on the microwave-assisted pyrolysis technique. Renew. Sust. Energ. Rev, 2013, 28, 317-330.

[8] Heuer A.H., Claussen N., Kriven W.M., Ruhle M., Stability of Tetragonal ZrO_2 Particles in Ceramic Matrices. J. Am. Ceram. Soc., 1982, 65(12), 642-650.

[9] Salema A.A., Afzal M.T., Numerical simulation of heating behaviour in biomass bed and pellets under multimode microwave system. Int. J. Thermal Sci., 2015, 91, 12-24.

[10] Guo S., Li W., Peng J., Niu H., Huang M., Zhang L., et al., Microwave-absorbing characteristics of mixtures of different carbonaceous reducing agents and oxidized ilmenite. Int. J. Miner. Process., 2009, 93(3-4), 289-293.

[11] Clemens J., Saltiel C., Numerical modeling of materials processing in microwave furnaces. Int. J. Heat. Mass Tran., 1996, 39(8), 1665-1675.

[12] Santos T., Valente M.A., Monteiro J., Sousa J., Costa L.C., Electromagnetic and thermal history during microwave heating. Appl. Therm. Eng., 2011, 31(16), 3255-3261.

[13] Chen X., Fan W., Study of the interaction between graphene and planar terahertz metamaterial with toroidal dipolar resonance. Opt. Lett., 2017, 42(10), 2034.

[14] Fanti A., Casu S., Desogus F., Montisci G., Simone M., Casula G.A., et al., Evaluation of a microwave resonant cavity as a reactor for enzyme reactions. J. Electromagnet. Wave., 2015, 29(17), 2380-2392.

[15] Halim S.A., Swithenbank J., Simulation study of parameters influencing microwave heating of biomass. J. Energy Inst., 2018, 92(4), 1191-1212.

[16] Salvi D., Boldor D., Aita G.M., Sabliov C.M., COMSOL Multiphysics model for continuous flow microwave heating of liquids. J. Food Eng., 2011, 104(3), 422-429.

[17] Chen J., Pitchai K., Birla S., Negahban M., Jones D., Subbiah J., Heat and Mass Transport during Microwave Heating of Mashed Potato in Domestic Oven-Model Development, Validation, and Sensitivity Analysis. J. Food Sci., 2014, 79(10), E1991-E2004.

[18] Leonelli C., Mason T.J., Microwave and ultrasonic processing: Now a realistic option for industry. Chem. Eng. Process., 2010, 49(9), 885-900.

[19] Choi W., Lee S.H., Kim C.T., Jun S., A finite element method based flow and heat transfer model of continuous flow microwave and ohmic combination heating for particulate foods. J. Food Eng., 2015, 149, 159-170.

[20] Li P., Luo F., Wang X., Zhou W., Zhu D., Effect of Y_2O_3 content on microwave dielectric properties of zirconia ceramics. Rare Metal Mat. Eng., 2007, 36(5), 623-626.

[21] Lin B., Li H., Chen Z., Zheng C., Hong Y., Wang Z., Sensitivity analysis on the microwave heating of coal: A coupled electromagnetic and heat transfer model. Appl. Therm. Eng., 2017, 126, 949-962.

[22] Salema A.A., Afzal M.T., Numerical simulation of heating behaviour in biomass bed and pellets under multimode microwave system. Int. J. Therm. Sci., 2015, 91, 12-24.

[23] He G., Qu W., Ju S., Liu C., Liu P., Wang S., et al., Effects of Temperature on Relaxation Time and Electrical Conductivity of Spent Automobile Catalyst at Microwave Frequencies. JOM, 2019, 71(7), 2353-2359.

[24] Ciacci T., Galgano A., Di Blasi C., Numerical simulation of the electromagnetic field and the heat and mass transfer processes during microwave-induced pyrolysis of a wood block. Chem. Eng. Sci., 65(14), 4117-4133.

[25] Tuta S., Koray Palazoğlu T., Finite element modeling of continuous-flow microwave heating of fluid foods and experimental validation. J. Food Eng., 2016, 192, 79-92.

[26] Mushtaq F., Channa A.S., Mat R., Ani F.N., Microwave Assisted Pyrolysis of Waste Biomass Resources for Bio-Oil Production. Appl. Mech. Mat., 2014, 554, 307-311.

[27] Robinson J.P., Kingman S.W., Lester E.H., Yi C., Microwave remediation of hydrocarbon-contaminated soils-scale-up using batch reactors. Sep. Purif. Technol., 2012, 96, 12-19.